Multichannel Quantum Defect Theory for cold molecular collisions

James F. E. Croft, Alisdair O. G. Wallis, and Jeremy M. Hutson

Department of Chemistry, Durham University, South Road, Durham, DH1 3LE, United Kingdom

Paul S. Julienne

Joint Quantum Institute, NIST and the University of Maryland, Gaithersburg, Maryland 20899-8423, USA

(Dated: August 30, 2011)

Multichannel Quantum Defect Theory (MQDT) is shown to be capable of producing quantitatively accurate results for low-energy atom-molecule scattering calculations. With a suitable choice of reference potential and short-range matching distance, it is possible to define a matrix that encapsulates the short-range collision dynamics and is only weakly dependent on energy and magnetic field. Once this has been produced, calculations at additional energies and fields can be performed at a computational cost that is proportional to the number of channels N and not to N^3. MQDT thus provides a promising method for carrying out low-energy molecular scattering calculations on systems where full exploration of the energy- and field-dependence is currently impractical.

PACS numbers:

Note for copy editor: We have been very careful to make correct use of Roman and italic subscripts and superscripts, with Roman for abbreviations and italic for mathematical indices. Please do not change all our subscripts and superscripts to italic. Also note that subscript lower-case o is an abbreviation for "open" and should not be changed to zero.

I. INTRODUCTION

The creation of the first dilute atomic Bose-Einstein condensates (BECs) in 1995 [1, 2] led to enormous advances in ultracold atomic physics. There is now great interest in producing samples of cold molecules, at temperatures below 1 K [3–5], and ultracold molecules, at temperatures below 1 mK [6–9]. There are many potential applications of ultracold molecular samples, amongst which are high-precision measurements [10, 11], quantum computation [12] and ultracold chemistry [13].

Understanding atomic and molecular interactions and collisions is essential to the study of cold and ultracold molecules. For example, methods such as buffer-gas cooling [14] and Stark deceleration [15] can produce cold molecules with temperatures between 10 mK and 1 K. However, a second-stage cooling method is needed to bring the molecules into the ultracold regime. Sympathetic cooling, in which the molecules are allowed to thermalize with a gas of ultracold atoms, is a promising second-stage cooling method [16]. However, while elastic collisions allow thermalization, inelastic collisions can cause trap loss [17], and for many systems the inelastic collisions are predicted to be too large for sympathetic cooling to succeed [18–20]. Scattering calculations are essential in order to identify systems for which sympathetic cooling has a good prospect of success. Once in the ultracold regime, the extent to which atomic and molecular interactions can be controlled again depends on a detailed understanding of their collisional properties.

Quantum molecular scattering calculations are usually carried out using the coupled-channel method: the Schrödinger equation for scattering is converted into a set of coupled differential equations, which are then propagated across a range of values of the intermolecular distance r. The size of the problem is determined by the number of channels N (the number of coupled equations). The usual algorithms take a time proportional to N^3, since each step of the propagation requires an $\mathcal{O}(N^3)$ matrix operation.

Cold molecule scattering presents problems with a large number of channels for two reasons:

1. At very low energies, small splittings between molecular energy levels become important. This makes it necessary to include fine details of molecular energy level patterns, such as tunneling and nuclear hyperfine splitting. The extra degrees of freedom require additional basis functions; in particular, including nuclear spins can multiply the number of equations by a substantial factor (sometimes 100 or more).

2. Collisions in the presence of electric and magnetic fields are very important. In an applied field, the total angular momentum J is no longer a good quantum number. Because of this, the large sets of coupled equations can no longer be factorized neatly into smaller blocks for each J as is possible in field-free scattering.

In addition, in cold molecule applications it is often necessary to repeat scattering calculations on a fine grid of energies and/or applied electric and magnetic fields, which adds greatly to the computational expense.

Multichannel Quantum Defect Theory (MQDT) offers an alternative to full coupled-channel calculations. It was originally developed to provide a uniform treatment of bound and scattering states for problems involving the interaction an electron with an ion core with

Coulomb forces at long range [21, 22], but was subsequently generalized to handle a range of other long-range potentials [22–27]. It has been successfully applied to scattering problems as diverse as negative ion photodetachment [28], near-threshold predissociation of diatomic molecules [25, 29] and predissociation of atom-diatom Van der Waals complexes [30, 31]. More recently it has been applied to ultracold collisions between pairs of neutral atoms [32–36], between atoms and ions [37, 38], and between highly reactive molecules [39–41].

MQDT can be viewed in two different ways. The first tries to capture the important physics of collisions within a few analytic quantum defect parameters. The other views it as a method for solving the coupled equations of scattering theory which offers substantial insights and advantages in efficiency. The common feature of the two approaches is to take advantage of the enormous difference in energy and length scales associated with separated collision partners and short-range potentials.

When MQDT is viewed as a numerical method for solving the coupled differential equations, the goal is to obtain a matrix $\boldsymbol{Y}(E, B)$ [24, 29, 34, 35] that completely describes the short-range dynamics and is insensitive to collision energy E and magnetic field B. This matrix can be obtained once and then used for calculations over a wide range of energies and fields, or obtained by interpolation from a few points. MQDT achieves this by defining $\boldsymbol{Y}(E, B)$ at relatively short range, as described below. The threshold behavior is accounted for from properties of single channels. Once the matrix $\boldsymbol{Y}(E, B)$ has been obtained, the time required for calculations at additional energies and fields is only proportional to N, not N^3.

Understanding threshold atomic physics in quantum defect terms is well developed [32–34, 42, 43]. Threshold bound-state and scattering properties are determined mainly by the long-range potential, which can often be approximated as $-C_n/r^n$. For the case of the Van der Waals interaction, $-C_6/r^6$, the linearly independent pair of solutions for a single potential is known [44]. An analytic approach to MQDT using these solutions has been developed [45, 46] and gives much insight into ultracold atom-atom collisions [47].

This paper investigates the use of MQDT as a numerical method to study cold atom-molecule collisions. The structure of the paper is as follows. In Section II we give an overview of the theory of MQDT, sufficient to define notation. In Section III we apply MQDT to the prototype system Mg+NH, and compare it with full coupled-channel calculations in order to establish what is required for it to give accurate results. In Section IV we present our conclusions and suggest directions for future work.

II. THEORY

A. Coupled-channel method

Cold atomic and molecular collisions and near-threshold bound states are conveniently described by a set of coupled equations. The Hamiltonian for an interacting pair of atoms or molecules is of the form

$$-\frac{\hbar^2}{2\mu}\nabla^2 + \hat{H}_{\text{int}}(\tau) + V(r, \tau), \qquad (1)$$

where μ is the reduced mass, ∇^2 is the Laplacian for the intermolecular coordinates, and τ denotes all coordinates except the interparticle distance r. $\hat{H}_{\text{int}}(\tau)$ represents the internal Hamiltonians of the two particles and $V(r, \tau)$ is the interaction potential. The total wavefunction is expanded

$$\Psi(r, \tau) = r^{-1} \sum_i \varphi_i(\tau) \psi_i(r), \qquad (2)$$

where the N functions $\varphi_i(\tau)$ form a basis set for the motion in all coordinates, τ, except the intermolecular distance, and $\psi_i(r)$ is the radial wavefunction in channel i. Substituting this expansion into the total time-independent Schrödinger equation and projecting onto the basis function $\varphi_j(\tau)$ yields the usual coupled equations of scattering theory,

$$\left[-\frac{\hbar^2}{2\mu}\frac{d^2}{dr^2} - E\right]\psi_j(r) = -\sum_i W_{ji}(r)\psi_i(r), \qquad (3)$$

where E is the energy. The coupling matrix $\boldsymbol{W}$ has elements

$$W_{ji}(r) = \int \varphi_j^*(\tau) \quad \left[H_{\text{int}}(\tau) + V(r, \tau) \right. $$
$$\left. + \frac{\hbar^2 L_i(L_i+1)}{2\mu r^2}\right]\varphi_i(\tau)\, d\tau, \quad (4)$$

where L_i is the partial-wave quantum number for channel i. Equation (3) can conveniently be written in matrix form,

$$\frac{\hbar^2}{2\mu}\frac{d^2\boldsymbol{\psi}}{dr^2} = [\boldsymbol{W}(r) - E\boldsymbol{I}]\boldsymbol{\psi}(r), \qquad (5)$$

where $\boldsymbol{\psi}(r)$ is a column vector made up of the solutions $\psi_i(r)$ and $\boldsymbol{I}$ is the identity matrix.

For both bound states and collision calculations, the wavefunction must be regular at the origin. When $V(r) \gg 0$ as $r \to 0$, the short-range boundary condition is

$$\psi_i(r) \to 0 \quad \text{as} \quad r \to 0. \qquad (6)$$

At any energy, there are N linearly independent solution vectors $\boldsymbol{\psi}(r)$ that satisfy these boundary conditions, and

it is convenient to combine them to form the $N \times N$ wavefunction matrix $\boldsymbol{\Psi}(r)$.

The coupled-channel approach propagates either the wavefunction matrix $\boldsymbol{\Psi}(r)$ and its derivative $\boldsymbol{\Psi}'(r)$, or the log-derivative matrix $\boldsymbol{L}(r) = \boldsymbol{\Psi}'[\boldsymbol{\Psi}]^{-1}$, outwards from $r = 0$ (or a point in the deeply classically forbidden region at short range) [48, 49]. In scattering calculations, the propagation is continued to a point $r_{\max}$ at large r. The wavefunction or log-derivative matrix is then transformed into a representation where $\boldsymbol{W}$ is asymptotically diagonal [50], such that

$$W_{ji}(r) \stackrel{r \to \infty}{\longrightarrow} \left[E_i^\infty + \frac{\hbar^2 L_i(L_i + 1)}{2\mu r^2} \right] \delta_{ij} + \mathcal{O}(r^{-n}), \quad (7)$$

where n is the power of the leading term in the potential expansion and E_i^∞ is the threshold of channel i. Each channel is either asymptotically open, $E \geq E_i^\infty$, or asymptotically closed, $E < E_i^\infty$. The scattering boundary conditions are

$$\boldsymbol{\Psi} = \boldsymbol{J}(r) + \boldsymbol{N}(r)\boldsymbol{K}. \quad (8)$$

The matrices $\boldsymbol{J}$ and $\boldsymbol{N}$ are diagonal matrices containing Riccati-Bessel functions for open channels and modified spherical Bessel functions for closed channels [49]. In a problem containing N channels, N_o of which are open, the scattering $\boldsymbol{S}$ matrix is related to the open-open sub-matrix of $\boldsymbol{K}$ by

$$\boldsymbol{S} = (1 + i\boldsymbol{K}_{oo})^{-1}(1 - i\boldsymbol{K}_{oo}). \quad (9)$$

In full coupled-channel calculations, the matrices $\boldsymbol{K}$ and $\boldsymbol{S}$ are rapidly changing functions of both energy and field, particularly near scattering resonances, so that the entire propagation to long range must be repeated for each set of conditions required.

B. Multichannel Quantum Defect Theory

MQDT also begins by propagating the wavefunction or log-derivative matrix outwards from short range. However, instead of continuing to $r_{\max}$, matching takes place at a point r_{match}, at relatively short range. The matching in MQDT treats the open and weakly closed channels on an equal footing; weakly closed channels are usually defined as those that are locally open, $E > W_{ii}(r)$, at some value of r, so are capable of supporting scattering resonances. Matching at short range produces a matrix $\boldsymbol{Y}(E, B)$ that is relatively insensitive to energy and applied field, as described below. $\boldsymbol{Y}$ also varies smoothly across thresholds, unlike $\boldsymbol{S}$ and $\boldsymbol{K}$. Provided the channels are uncoupled outside r_{match}, it is then possible to obtain the scattering $\boldsymbol{S}$ matrix from $\boldsymbol{Y}$ using the properties of individual uncoupled channels.

We consider a problem with N_o open channels and N_c weakly closed channels at some collision energy E and field B. For each such channel, $i = 1, N$, where $N =$ $N_o + N_c$, MQDT requires a reference potential, $U_i^{\mathrm{ref}}(r)$, which asymptotically has similar behavior to $W_{ii}(r)$ in equation (7). This reference potential defines a linearly independent pair of reference functions $f_i(r)$ and $g_i(r)$,

$$\left[\frac{d^2}{dr^2} + K_i^2(r) \right] f_i(r) = 0, \quad (10)$$

and similarly for g_i, where the local wave vector $K_i(r)$ is

$$K_i(r) = \sqrt{\frac{2\mu}{\hbar^2}(E - U_i^{\mathrm{ref}}(r))}. \quad (11)$$

The regular solution f_i has the boundary condition $f_i \to 0$ as $r \to 0$. f_i and g_i are normalized to have Wentzel-Kramers-Brillouin (WKB) form, with amplitude $K_i(r)^{-1/2}$, at some point in the classically allowed region [24]. The $N \times N$ matrix $\boldsymbol{Y}$ is defined by matching at r_{match},

$$\boldsymbol{\Psi} = \boldsymbol{f}(r) + \boldsymbol{g}(r)\boldsymbol{Y}, \quad (12)$$

or in terms of the log-derivative matrix $\boldsymbol{L}$,

$$(\boldsymbol{L}\boldsymbol{f} - \boldsymbol{f}') = (\boldsymbol{L}\boldsymbol{g} - \boldsymbol{g}')\boldsymbol{Y}, \quad (13)$$

where $\boldsymbol{f}$ and $\boldsymbol{g}$ are diagonal matrices containing the functions f_i and g_i and the primes indicate radial derivatives.

In order to relate $\boldsymbol{Y}$ to the physical scattering $\boldsymbol{S}$ matrix, the asymptotic forms of the reference functions f_i and g_i in each channel are required. To this end another pair of reference functions is defined for each channel. For open channels, these functions are asymptotically energy-normalized,

$$s_i(r) \stackrel{r \to \infty}{\longrightarrow} k_i^{-\frac{1}{2}} \sin\left(k_i r - \frac{L_i \pi}{2} + \xi_i\right), \quad (14)$$

$$c_i(r) \stackrel{r \to \infty}{\longrightarrow} k_i^{-\frac{1}{2}} \cos\left(k_i r - \frac{L_i \pi}{2} + \xi_i\right), \quad (15)$$

where ξ_i is the phase shift associated with reference potential i and k_i is the asymptotic wave vector,

$$k_i = \sqrt{\frac{2\mu}{\hbar^2}(E - E_i^\infty)}. \quad (16)$$

These asymptotically normalized functions are related to f_i and g_i through the quantum defect parameters C_i and $\tan \lambda_i$,

$$s_i(r) = C_i^{-1} f_i(r); \quad (17)$$
$$c_i(r) = C_i[g_i(r) + \tan \lambda_i f_i(r)]. \quad (18)$$

Thus C_i relates the amplitudes of the energy-normalised reference functions to WKB-normalised ones, while $\tan \lambda_i$ describes the modification in phase due to threshold effects. Far from threshold, $C_i \approx 1$ and $\tan \lambda_i \approx 0$.

For each weakly closed channel, an exponentially decaying solution is defined,

$$\phi_i(r) \stackrel{r \to \infty}{\longrightarrow} \tfrac{1}{2} e^{-|k_i|r} \sqrt{|k_i|}. \quad (19)$$

This is related to the solutions f_i and g_i by a normalization factor $\mathcal{N}_i$, and an energy-dependent phase ν_i,

$$\phi_i(r) = \mathcal{N}_i \left[\cos\nu_i f_i(r) - \sin\nu_i g_i(r)\right]. \qquad (20)$$

The phase ν_i is an integer multiple of π at each energy that corresponds to a bound state of the reference potential in channel i.

The $\boldsymbol{Y}$ matrix is converted into the $\boldsymbol{S}$ matrix of scattering theory using the quantum defect parameters C_i, $\tan\lambda_i$, $\tan\nu_i$ and ξ_i. First, the effect of coupling to closed channels is accounted for,

$$\overline{\boldsymbol{Y}} = \boldsymbol{Y}_{\text{oo}} - \boldsymbol{Y}_{\text{oc}}[\tan\boldsymbol{\nu} + \boldsymbol{Y}_{\text{cc}}]^{-1}\boldsymbol{Y}_{\text{co}}, \qquad (21)$$

where $\tan\boldsymbol{\nu}$ is a diagonal matrix of dimension $N_{\text{c}} \times N_{\text{c}}$ containing elements $\tan\nu_i$. The $N_{\text{o}} \times N_{\text{o}}$ matrix $\overline{\boldsymbol{Y}}$ incorporates any resonance structure caused by coupling to closed channels through $\tan\boldsymbol{\nu}$. Unlike $\boldsymbol{Y}$ itself, $\overline{\boldsymbol{Y}}$ can be a rapidly varying function of energy and field. Secondly, threshold effects from asymptotically open channels are incorporated,

$$\overline{\boldsymbol{R}} = \boldsymbol{C}^{-1}\left[\overline{\boldsymbol{Y}}^{-1} - \tan\boldsymbol{\lambda}\right]^{-1}\boldsymbol{C}^{-1}, \qquad (22)$$

where $\boldsymbol{C}$ and $\tan\boldsymbol{\lambda}$ are diagonal matrices of dimension $N_{\text{o}} \times N_{\text{o}}$, containing elements C_i and $\tan\lambda_i$. Finally, the $\boldsymbol{S}$ matrix is obtained from

$$\boldsymbol{S} = e^{i\boldsymbol{\xi}}\left[1 + i\overline{\boldsymbol{R}}\right]\left[1 - i\overline{\boldsymbol{R}}\right]^{-1}e^{i\boldsymbol{\xi}}. \qquad (23)$$

This may be compared to equation (9) for the full coupled-channel method. The inclusion of the diagonal matrix $e^{i\boldsymbol{\xi}}$ accounts for the phase difference between the reference functions f_i and g_i used by MQDT and the Riccati-Bessel functions used by the full coupled-channel method.

The approach taken in the present paper is somewhat different from that in refs. [25, 34]. There MQDT was approached as an exact representation of the full coupled-channel solution. The matrix $\boldsymbol{Y}$ was evaluated at a distance r_{match} large enough that it had become constant as a function of r_{match}. When this is done, MQDT gives the same (exact) results for any choice of reference potential $U_i^{\text{ref}}(r)$, although constancy of $\boldsymbol{Y}$ may be achieved at different values of r_{match} for different choices. In our approach, r_{match} is chosen to ensure that $\boldsymbol{Y}$ is only weakly energy-dependent, and this may require matching in a region where $\boldsymbol{Y}$ is not yet independent of r_{match}. With this approach, MQDT provides an *approximate* solution whose quality depends on the choice of reference potentials.

C. Numerical evaluation of reference functions and quantum defect parameters

1. Open channels

For an open channel i, the reference function s_i is obtained by propagating a regular solution of (10) from a point inside r_{match} to a point r_{max} at long range and imposing the boundary condition (14) (or its Bessel function equivalent). This establishes the normalization of s_i and also gives the phase shift ξ_i, which is then used to obtain the function c_i at r_{max} from the boundary condition (15). The reference function c_i is then propagated inwards to r_{match}. The two remaining quantum defect parameters are obtained by applying [25]

$$C_i^{-2} = (s_i^2 K_i + s_i'^2/K_i) \qquad (24)$$

and

$$\cot\lambda_i = \frac{K_i(\gamma_i - u_i)}{K_i^2 + \gamma_i u_i} \qquad (25)$$

in the classically allowed region, where $\gamma_i = s_i'/s_i$ and $u_i = c_i'/c_i$. The primes indicate radial derivatives. Equations (17) and (18) then give the reference functions f_i and g_i.

2. Closed channels

For a weakly closed channel i, the reference function f_i is again obtained by propagating a regular solution of (10) outwards from a point inside r_{match}, but in this case f_i is normalized in the classically allowed region such that

$$f_i^2(K_i^2 + \gamma_i^2) = K_i. \qquad (26)$$

In the closed-channel case, g_i cannot be obtained directly from f_i at a single point. Instead, the reference function ϕ_i is obtained by using (19) as a long-range boundary condition and propagating a solution of (10) inwards towards $r = 0$. The normalization factor $\mathcal{N}_i$ of equation (20) is obtained by matching to

$$\mathcal{N}_i^2 = (\phi_i^2 K_i + \phi_i'^2/K_i). \qquad (27)$$

in the classically allowed region. The quantum defect parameter $\tan\nu_i$ is then obtained from

$$\tan\nu_i = \frac{K_i(t_i - \gamma_i)}{K_i^2 + \gamma_i t_i}, \qquad (28)$$

where $t_i = \phi_i'/\phi_i$. Finally, the function g_i is obtained from f_i and ϕ_i using equation (20).

D. Sources of Error

There are a number of sources of errors in MQDT calculations using our approach:

1. Interchannel couplings that occur outside r_{match}, which are not taken into account by equations (21) to (23);

2. Deviations between the reference potentials $U_i^{\text{ref}}(r)$ and $W_{ii}(r)$ outside r_{match};

3. Differences between the actual $\boldsymbol{Y}$ matrix at a given energy and field and the $\boldsymbol{Y}$ matrix obtained by interpolation.

III.   RESULTS AND DISCUSSION

To explore the application of MQDT to cold molecular collisions, we consider the prototype system Mg+NH($^3\Sigma^-$). The potential energy surface for this system is moderately anisotropic [51] and provides substantial coupling between channels. The system is topical because Wallis and Hutson [52] have shown that sympathetic cooling of cold NH molecules by ultracold Mg atoms has a good prospect of success.

The energy levels of NH in a magnetic field are most conveniently described using Hund's case (b), in which the molecular rotation n couples to the spin s to produce a total monomer angular momentum j. In zero field, each rotational level n is split into sublevels labeled by j. In a magnetic field, each sublevel splits further into $2j + 1$ levels labeled by m_j, the projection of j onto the axis defined by the field. For the $n = 0$ levels that are of most interest for cold molecule studies, there is only a single zero-field level with $j = 1$ that splits into three components with $m_j = +1$, 0 and -1.

The coupled equations are constructed in a partly coupled basis set $|nsjm_j\rangle|LM_L\rangle$, where L is the end-over-end rotational angular momentum of the Mg atom and the NH molecule about one another and M_L is its projection on the axis defined by the magnetic field. Hyperfine structure is neglected. The matrix elements of the total Hamiltonian in this basis are given in ref. [50]. The only good quantum numbers during the collision are the parity $p = (-1)^{n+L+1}$ and the total projection quantum number $M = m_j + M_L$. The calculations in the present work are performed for $p = -1$ and $M = 1$. This choice includes s-wave scattering of NH molecules in initial state $m_j = +1$, which is magnetically trappable, to $m_j = 0$ and -1, which are not. The basis set used included all functions up to $n_{max} = 1$ and $L_{max} = 3$. This unconverged basis set is sufficient for the purpose of comparing MQDT results with full coupled-channel calculations.

A.   Numerical methods

The coupled-channel calculations required for both MQDT and the full coupled-channel approach were carried out using the MOLSCAT package [53], as modified to handle collisions in magnetic fields [50]. The coupled equations were solved numerically using the hybrid log-derivative propagator of Alexander and Manolopoulos [54], which uses a fixed-step-size log-derivative propagator in the short-range region ($r_{min} \leq r < r_{mid}$) and a variable-step-size Airy propagator in long-range region ($r_{mid} \leq r \leq r_{max}$. The full coupled-channel calculations used $r_{min} = 2.5$ Å, $r_{mid} = 50$ Å and $r_{max} = 250$ Å (where 1 Å $= 10^{-10}$ m). MQDT requires coupled-channel calculations only from r_{min} to r_{match} (which is less than r_{mid}), so only the fixed-step-size propagator was used in this case.

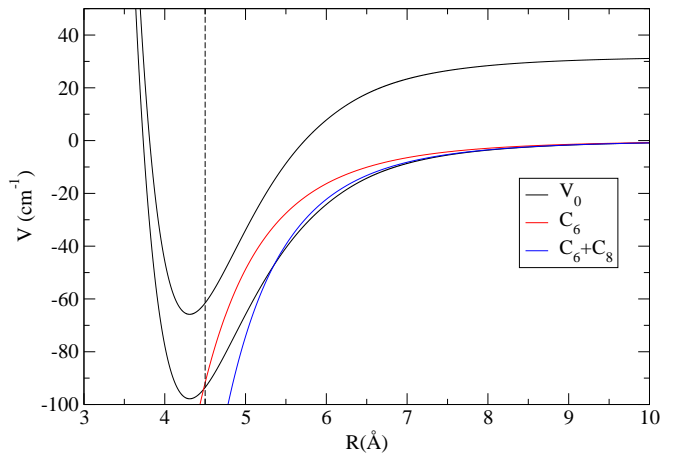The MQDT reference functions and quantum defect

FIG. 1: (Color online) Zero-field reference potentials. For the V_0 reference potential the first rotational excited state is also shown ($n = 1$). The hard wall at $r = 4.5$ Å is shown as a dashed line.

parameters were obtained as described in Section II C, using the Numerov propagator [55] to solve the 1-dimension Schrödinger equations. Use of the renormalized Numerov method [56] was not found to be necessary in the present case. The MQDT $\boldsymbol{Y}$ matrix was then obtained by matching to the log-derivative matrix extracted from the coupled-channel propagation at a distance r_{match}.

B.   Comparison of full coupled-channel and MQDT results

1.   Choice of r_{match} and reference potential

One of the goals of MQDT is to obtain a matrix $\boldsymbol{Y}(E, B)$ in such a way that it is only weakly dependent on energy E and magnetic field B. However, the actual form of $\boldsymbol{Y}(E, B)$ is strongly dependent on the distance at which it is defined and the reference potentials used. In the present work we consider three different reference potentials, as shown in Figure 1. First we define a reference potential containing a pure C_6 long-range term, which has been used with great success in cold atom-atom collisions,

$$U_i^{\text{ref},C_6}(r) = -\frac{C_6}{r^6} + \frac{\hbar^2 L_i(L_i + 1)}{2\mu r^2} + E_i^\infty, \qquad (29)$$

where $C_6 = 7.621 \times 10^5$ Å^6 cm^{-1} for Mg+NH [51]. Secondly we define a reference potential containing an additional C_8 term,

$$U_i^{\text{ref},C_{6,8}}(r) = -\frac{C_6}{r^6} - \frac{C_8}{r^8} + \frac{\hbar^2 L_i(L_i + 1)}{2\mu r^2} + E_i^\infty, \quad (30)$$

where $C_8 = 9.941 \times 10^6$ Å^8 cm^{-1} [51]. Finally we define

$$U_i^{\text{ref},V_0}(r) = V_0(r) + \frac{\hbar^2 L_i(L_i + 1)}{2\mu r^2} + E_i^\infty, \qquad (31)$$
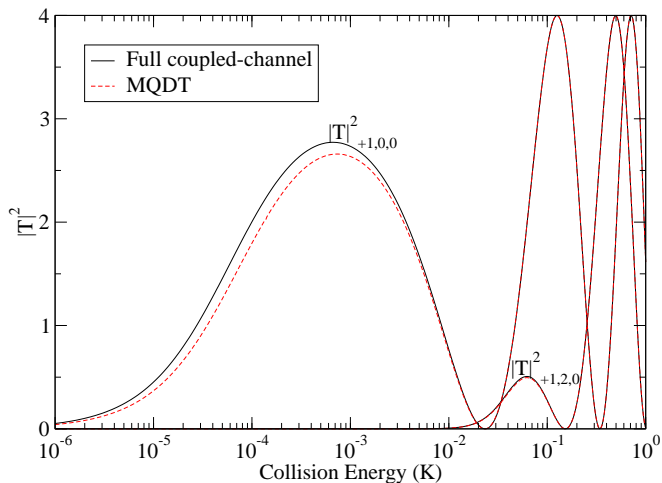
FIG. 2: (Color online) The squares of diagonal T-matrix elements in the incoming channels for $m_j = +1$, $L = 0$ and 2 at $B = 10$ G, obtained from full coupled-channel calculations (solid, black) and MQDT with the C_6 reference potential and $r_{\mathrm{match}} = 20$ Å (dashed, red). T-matrix elements are labeled with quantum numbers m_j, L, M_L. [Units of Gauss rather than Tesla, the accepted SI unit of magnetic field, have been used in this paper to conform to the conventional usage of this field.]
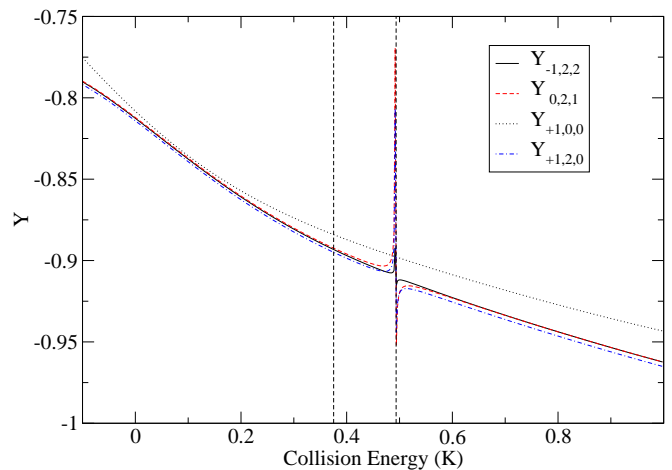

FIG. 3: (Color online) Diagonal Y matrix elements as a function of collision energy at $B = 10$ G for the C_6 reference potential with $r_{\mathrm{match}} = 20$ Å. The dashed vertical lines show the positions of quasibound states as described in the text.

where $V_0(r)$ is the isotropic part of the interaction potential, which is equivalent to the diagonal $\boldsymbol{W}$ matrix element in the incoming s-wave channel. Each reference potential contains a hard wall at $r = r_i^{\mathrm{wall}}$, so that $U_i^{\mathrm{ref}}(r) = \infty$ for $r < r_i^{\mathrm{wall}}$. This allows the phase ξ_i of the reference functions in each channel to be adjusted if required. A useful feature of MQDT, to be explored in future work, is that the position of the hard wall can be chosen to minimize the energy-dependence of $\boldsymbol{Y}$. However, in the present paper we simply take $r_i^{\mathrm{wall}} = 4.5$ Å.

It is convenient to compare MQDT and coupled-channel results at the level of T-matrix elements, $T_{ij} = \delta_{ij} - S_{ij}$. In general we label elements $T_{\alpha,L,M_L \to \alpha',L',M_L'}$, where $|\alpha\rangle = |nsjm_j\rangle$. However, the collisions considered in the present paper are all among the $n = 0, j = 1$ levels and so α is simply abbreviated to m_j. The spin-changing cross sections are quite small except near resonances, so we focus mostly on diagonal elements, for which we suppress the second set of labels.

Figure 2 compares diagonal T-matrix elements $|T_{ii}|^2$ obtained from full coupled-channel calculations with those from the MQDT method for the pure C_6 reference potential of equation (29), with a matching distance of $r_{\mathrm{match}} = 20$ Å. The $\boldsymbol{Y}$ matrix was recalculated at every energy at which full coupled-channel calculations were performed. The MQDT results reproduce the coupled-channel results almost exactly at collision energies $E/k_{\mathrm{B}} > 10$ mK. However, at lower energies the results start to differ noticeably. It may be noted that $|U_i^{\mathrm{ref},C_6} - W_{ii}|/k_{\mathrm{B}} \approx 0.6$ mK at $r_{\mathrm{match}} = 20$ Å.

Figure 3 shows the diagonal $\boldsymbol{Y}$ elements correspond-

ing to Figure 2. They vary smoothly across most of the energy range, and are continuous across the threshold at zero energy, but exhibit occasional sharp structures as a function of energy. These sharp features are close to the energies of quasibound states, as shown by carrying out bound-state calculations using the BOUND package [57], with the same basis set as the MOLSCAT calculations. The resulting bound-state energies are shown in Figure 3 as dashed vertical lines. The broad feature near $E/k_{\mathrm{B}} = 0.5$ K is due to a quasibound state (Feshbach resonance) with quantum numbers $n = 1$, $j = 0$, $m_j = 0$, $L = 3$.

For MQDT to be more efficient than full coupled-channel calculations, it needs to produce results in agreement with full coupled-channel calculations from an energy-insensitive $\boldsymbol{Y}$ matrix that can be assumed to be constant or can be obtained by interpolation from a few energies, instead of being recalculated at every energy. However, the $\boldsymbol{Y}$ matrix elements in Figure 3 do not meet this requirement: the resonant features prevent reliable interpolation over useful ranges of energy.

The energy sensitivity of the $\boldsymbol{Y}$ matrix in Figure 3 is due to the value used for r_{match}. When r_{match} is large, resonance features due to quasibound states may be present in the log-derivative matrix from which $\boldsymbol{Y}$ is obtained. In this case the open and closed-channel blocks of $\boldsymbol{Y}$ are uncoupled, so that $\bar{\boldsymbol{Y}} \approx \boldsymbol{Y}_{\mathrm{oo}}$, and the resonances appear through the $\boldsymbol{Y}_{\mathrm{oo}}$ term in Eq. 21 rather than through $\tan \boldsymbol{\nu} + \boldsymbol{Y}_{\mathrm{cc}}$ [58]. However, if r_{match} is small enough, the resonance features are shifted to high energies, out of the region of interest. It is usually desirable to obtain $\boldsymbol{Y}$ at a value of r_{match} that is in or near the classically allowed region for all weakly closed channels. However it must be remembered that the MQDT method neglects interchannel couplings that occur outside r_{match}, so there is always a tradeoff between choosing
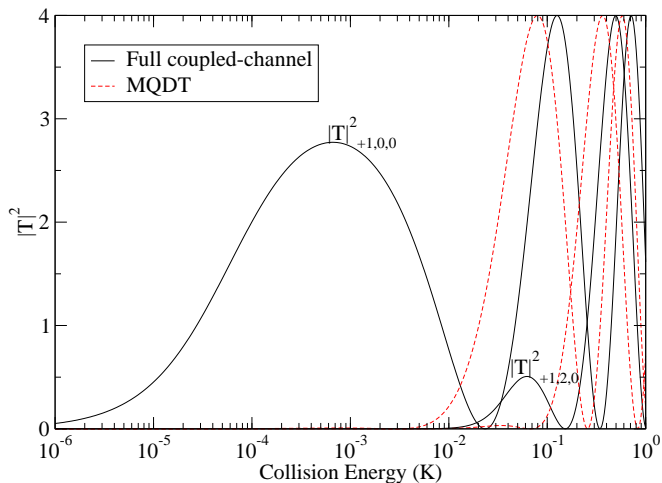
FIG. 4: (Color online) The squares of diagonal T-matrix elements in the incoming channels for $m_j = +1$, $L = 0$ and 2 at $B = 10$ G, obtained from full coupled-channel calculations (solid, black) and MQDT with the C_6 reference potential and $r_{\mathrm{match}} = 6.8$ Å (dashed, red).

FIG. 5: (Color online) The squares of diagonal T-matrix elements in the incoming channels for $m_j = +1$, $L = 0$ and 2 at $B = 10$ G, obtained from full coupled-channel calculations (solid, black) and MQDT with the $C_6 + C_8$ (dot-dashed, blue) and V_0 (dashed, red) reference potentials and $r_{\mathrm{match}} = 6.8$ Å.

a value that minimizes the energy-dependence and one that takes account of coupling at relatively long range. This is particularly important in molecular scattering, where the anisotropy of the interaction potential often provides substantial couplings at long range.

It is convenient to consider lengths and energies in ultracold scattering in relation to the Van der Waals characteristic length and energy, defined by [59]

$$r_{\mathrm{VdW}} = \frac{1}{2}\left(\frac{2\mu C_6}{\hbar^2}\right)^{\frac{1}{4}} \quad \text{and} \quad E_{\mathrm{VdW}} = \frac{\hbar^2}{2\mu r_{\mathrm{VdW}}^2}. \quad (32)$$

For Mg+NH, $r_{\mathrm{VdW}} = 12.7$ Å and $E_{\mathrm{VdW}}/k_B = 11$ mK. In atomic systems, it is common to place r_{match} close to r_{VdW}. However, the quasibound state responsible for the broad feature in Figure 3 is due to an $n = 1$ state, with an outer turning point around 5.7 Å. The resonant feature therefore does not shift in energy significantly until r_{match} is around 7 Å. In addition, it is not enough simply to move r_{match} to short range with the same reference function. Figure 4 shows diagonal T-matrix elements obtained by MQDT with the C_6 reference function, as in Figure 2, but with $r_{\mathrm{match}} = 6.8$ Å. This does indeed produce a $\boldsymbol{Y}$ matrix without poles in the energy region of interest, but the MQDT results are no longer in agreement with the full coupled-channel results at any of the energies considered. This is because the difference between the reference potential and the diagonal $\boldsymbol{W}$ matrix elements at $r_{\mathrm{match}} = 6.8$ Å is $|U_i^{\mathrm{ref},C_6} - W_{ii}|/k_B \approx 4$ K, as seen in Figure 1. Alternatively, in terms of the approach of Mies and Raoult [34], 6.8 Å is too short a distance for the $\boldsymbol{Y}$ matrix evaluated with the C_6 reference potential to have reached its asymptotic value.

This problem may be remedied by using a better reference potential. Figure 5 shows results obtained using
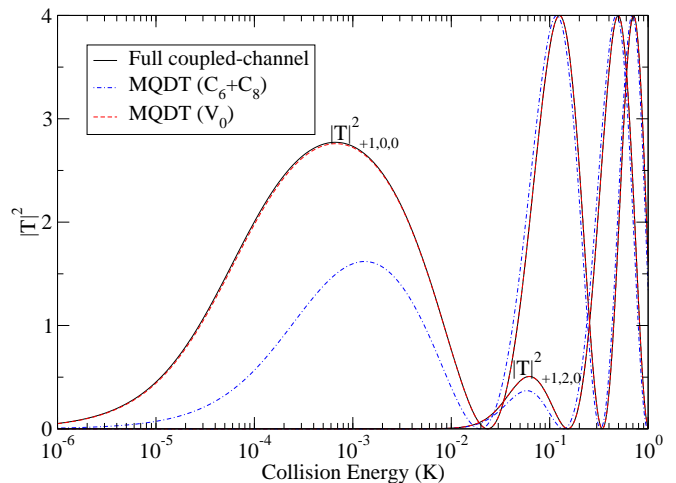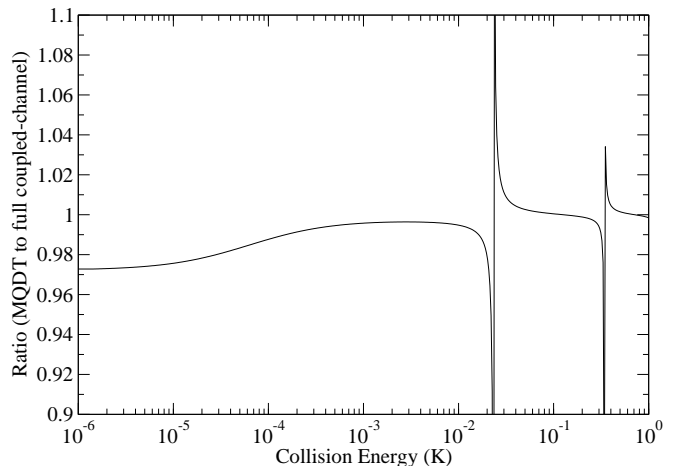

FIG. 6: Ratio of the square of the diagonal $\boldsymbol{T}$ matrix element for $m_j = +1$, $L = 0$ at $B = 10$ G for MQDT, with the V_0 reference potential and $r_{\mathrm{match}} = 6.8$ Å, to that from full coupled-channel calculations.

the reference potentials of equations (30) and (31), again for $r_{\mathrm{match}} = 6.8$ Å. The $C_6 + C_8$ reference potential gives a marked improvement over the pure C_6 reference potential. The $\boldsymbol{T}$ matrix elements it produces follow the form of the full coupled-channel results but still become poor at energies much below 1 K: at $r_{\mathrm{match}} = 6.8$ Å, $|U_i^{\mathrm{ref},C_6+C_8} - W_{ii}|/k_B \approx 0.35$ K. However, the results obtained with the V_0 reference potential are much more accurate, and can scarcely be distinguished from the full coupled-channel results in Figure 5.

Even the V_0 reference potential does not produce exact results. Figure 6 shows the ratio of the MQDT T-matrix elements for this reference potential to the full coupled-channel results. The poles in the ratio arise sim-
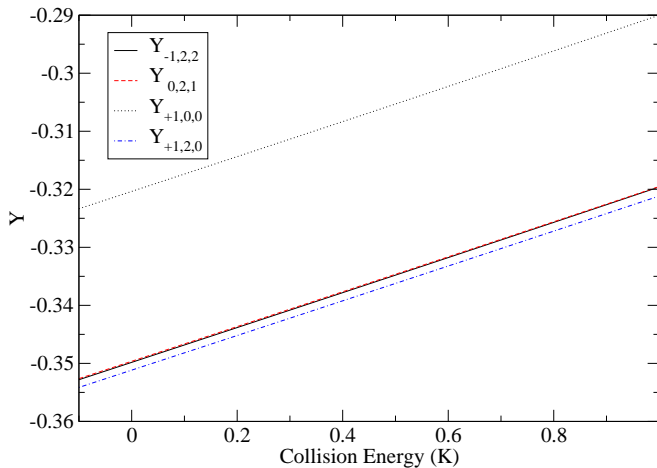
FIG. 7: (Color online) Diagonal $\boldsymbol{Y}$ matrix elements as a function of energy at $B = 10$ G, for the V_0 reference potential with $r_{\text{match}} = 6.8$ Å.

FIG. 8: (Color online) Diagonal $\boldsymbol{Y}$ matrix elements as a function of magnetic field at $E/k_{\text{B}} = 400$ mK, for the V_0 reference potential with $r_{\text{match}} = 6.8$ Å.

ply because MQDT places the zeroes in $|T|^2$ (where the phase shift is an integer multiple of π) at very slightly different collision energies. However, at very low energies (below about 1 mK) the MQDT results underestimate the squared T-matrix elements by up to 3%. This probably arises because the "best" reference potential would be one that takes account of adiabatic shifts due to mixing in excited rotational levels. For the $n = 0$ channels, the shift due to $n = 1$ channels may be estimated from 2nd-order perturbation theory to be about 0.012 cm^{-1} (equivalent to 17 mK) at $r_{\text{match}} = 6.8$ Å. This will cause residual errors in the MQDT C functions that are responsible for the small errors visible in Figure 6.

Figure 7 shows representative matrix elements of $\boldsymbol{Y}$ obtained at $r_{\text{match}} = 6.8$ Å, with the V_0 reference potential, as a function of energy. It may be seen that they are nearly linear in energy. The other matrix elements of $\boldsymbol{Y}$ show similar behavior. While the actual values of matrix elements vary substantially, they are all nearly linear in energy for $r_{\text{match}} = 6.8$ Å.

It should be noted that when the reference functions are obtained numerically, as in the present work, there is no significant difference in computer time for different choices of reference potential. Using the full V_0 reference potential is just as inexpensive as using a simpler one.

2. Feshbach resonances

Magnetic fields have important effects on cold molecular collisions, and in particular magnetically tunable low-energy Feshbach resonances provide mechanisms by which the collisions may be *controlled*. It is therefore important to establish whether the $\boldsymbol{Y}$ matrices obtained from MQDT are smooth functions of magnetic field as well as energy and can be used to characterize Feshbach resonances. If they are, it will offer substantial compu-
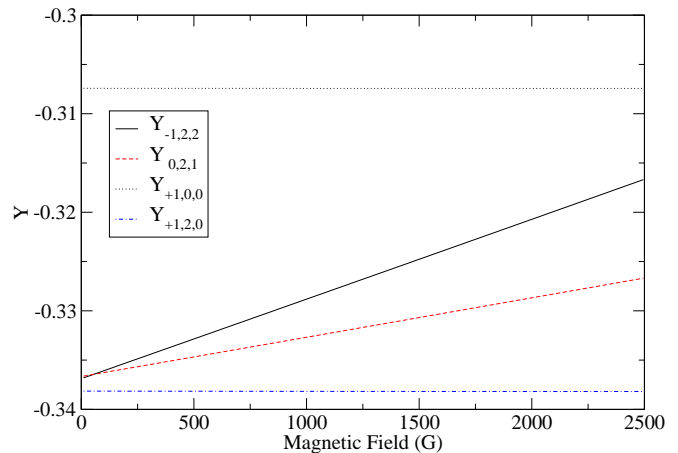
tational efficiencies.

Figure 8 shows how the diagonal $\boldsymbol{Y}$ matrix elements vary as a function of magnetic field for Mg+NH collisions over the range from 0 to 2500 G for a collision energy of 400 mK. It may be seen that the matrix elements are indeed very nearly linear, as required for efficient interpolation.

In Mg+NH, there is a Feshbach resonance due to the $n = 1$, $j = 0$, $m_j = 0$, $L = 3$ state shown in Figure 3 that tunes down towards the $n = 0$, $m_j = +1$ threshold with increasing field. Figure 9 shows the comparison between MQDT and full coupled-channel calculations for a selection of diagonal and off-diagonal $\boldsymbol{T}$ matrix elements as the magnetic field is tuned across this resonance at energies of 400 mK and 1 mK. At each energy, MQDT results were obtained both by recalculating the $\boldsymbol{Y}$ matrix at every field and by linear interpolation between two points separated by 100 G. In both cases, the interpolated MQDT results are within about 0.2 G of the full MQDT results even for this long interpolation, and this could of course be improved simply by considering a few more fields across the range to allow. However, there is also a residual error of of 0.1 to 0.2 G in the resonance position even for the full MQDT results, which is not very different at the two collision energies considered. This is again likely to be due to the effect as described in Section III B 1: the V_0 reference potential neglects couplings between channels outside r_{match}, and for the small value of r_{match} used here these couplings are sufficient to shift the resonance positions slightly. Apart from these small shifts, however, both the elastic and the inelastic scattering around the resonances are very well described at both energies.

The linearity of the $\boldsymbol{Y}$ matrix with both energy and applied magnetic field is an extremely promising result, and suggests that MQDT will provide very efficient ways of performing cold collision calculations as a function of energy and magnetic field, without needing to repeat the
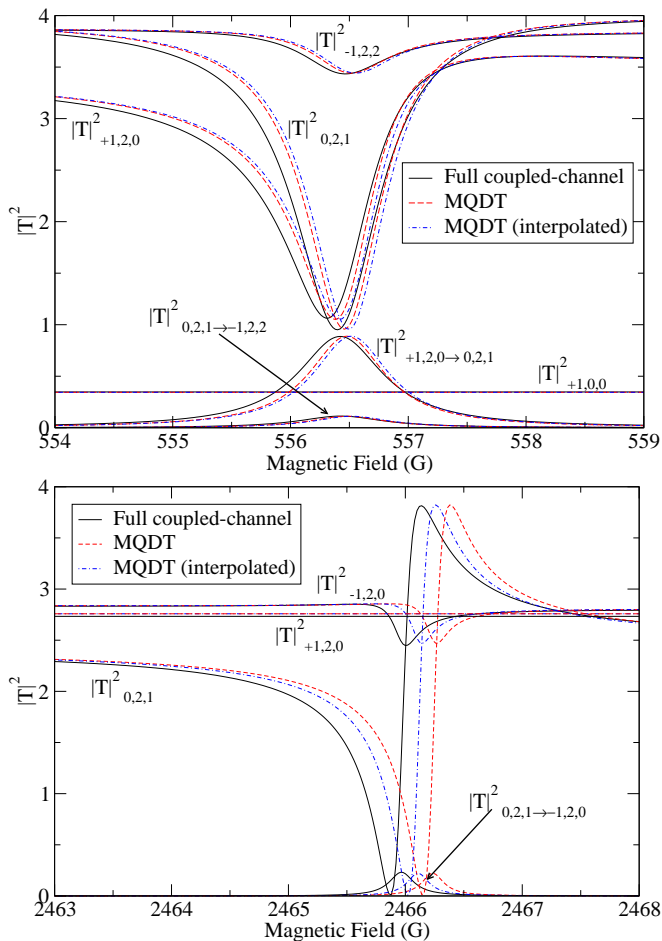
FIG. 9: (Color online) Squares of diagonal and off-diagonal T-matrix elements as the field is tuned across a Feshbach resonance at $E/k_{\mathrm{B}} = 400$ mK (upper panel) and 1 mK (lower panel). The MQDT results are obtained with the V_0 reference potential at $r_{\mathrm{match}} = 6.8$ Å.

expensive coupled-channel part of the calculation on a fine grid.

IV. CONCLUSIONS

We have shown that Multichannel Quantum Defect Theory (MQDT) can be applied to low-energy molecular collisions in applied magnetic fields. MQDT provides a matrix $\boldsymbol{Y}$, defined at a distance r_{match} at relatively short range, which encapsulates all the short-range dynamics of the system. For the prototype Mg+NH system, we have shown that MQDT can provide numerical results that

are in quantitative agreement with full coupled-channel calculations if the MQDT reference functions are defined appropriately.

We have investigated the effect of different choices of reference potential and values of r_{match}. For cold atom-molecule collisions, unlike cold atom-atom collisions, calculations are likely to be needed over a significant range of collision energy, perhaps 1 K or so. If r_{match} is placed at too long a range, there is a significant likelihood of resonant features within the energy range that prevent simple interpolation of $\boldsymbol{Y}$. This may be circumvented by carrying out the matching at a smaller distance r_{match}. However, when this is done, a pure C_6 reference potential may not be sufficient. For Mg+NH, the most satisfactory procedure is to perform matching at fairly short range (inside 7 Å) and use a reference potential that is defined to be the same as the true diagonal potential in the incoming channel.

The major strength of MQDT for molecular applications is that, if the the matching to obtain $\boldsymbol{Y}$ is carried out at relatively short range, the matrix is only weakly dependent on collision energy and magnetic field. This allows very considerable computational efficiencies, because the expensive calculation to obtain $\boldsymbol{Y}$ needs to be carried out at only one or a few combinations of collision energy and field. The remaining calculations to obtain scattering properties on a fine grid of energies and fields are then computationally inexpensive, varying only linearly with the number of channels N. Full coupled-channel calculations, by contrast, scale as N^3.

MQDT is a promising alternative to full coupled-channel calculations for cold atom-molecule collisions, particularly when fine scans over collision energy and magnetic field are required. In future work, we will investigate further the choice of reference functions to optimize the accuracy and to minimize the dependence of $\boldsymbol{Y}$ on collision energy and field. We will also investigate how the results for Mg+NH transfer to more strongly anisotropic systems, with stronger long-range anisotropy and more closed channels that are capable of producing scattering resonances.

V. ACKNOWLEDGMENTS

[1] M. H. Anderson, J. R. Ensher, M. R. Matthews, C. E. Wieman, and E. A. Cornell, Science **269**, 198 (1995).

[2] K. B. Davis, M.-O. Mewes, M. R. Andrews, N. J. van Druten, D. S. Durfee, D. M. Kurn, and W. Ketterle, Phys. Rev. Lett. **75**, 3969 (1995).

[3] J. Doyle, B. Friedrich, R. V. Krems, and F. Masnou-

Seeuws, Eur. Phys. J. D **31**, 149 (2004).

[4] R. V. Krems, Int. Rev. Phys. Chem. **24**, 99 (2005).

[5] B. Friedrich and J. M. Doyle, ChemPhysChem **10**, 604 (2009).

[6] J. M. Hutson and P. Soldán, Int. Rev. Phys. Chem. **25**, 497 (2006).

[7] K.-K. Ni, S. Ospelkaus, M. H. G. de Miranda, A. Pe'er, B. Neyenhuis, J. J. Zirbel, S. Kotochigova, P. S. Julienne, D. S. Jin, and J. Ye, Science **322**, 231 (2008).

[8] S. Ospelkaus, K.-K. Ni, D. Wang, M. H. G. de Miranda, B. Neyenhuis, G. Quéméner, P. S. Julienne, J. L. Bohn, D. S. Jin, and J. Ye, Science **327**, 853 (2010).

[9] J. G. Danzl, M. J. Mark, E. Haller, M. Gustavsson, R. Hart, J. Aldegunde, J. M. Hutson, and H.-C. Nägerl, Nature Phys. **6**, 265 (2010).

[10] J. J. Hudson, B. E. Sauer, M. R. Tarbutt, and E. A. Hinds, Phys. Rev. Lett. **89**, 023003 (2002).

[11] H. L. Bethlem and W. Ubachs, Faraday Discuss. **142**, 25 (2009).

[12] D. DeMille, Phys. Rev. Lett. **88**, 067901 (2002).

[13] M. Bell and T. P. Softley, Mol. Phys. **107**, 99 (2009).

[14] J. D. Weinstein, R. deCarvalho, T. Guillet, B. Friedrich, and J. M. Doyle, Nature **395**, 148 (1998).

[15] H. L. Bethlem and G. Meijer, Int. Rev. Phys. Chem. **22**, 73 (2003).

[16] P. Soldán and J. M. Hutson, Phys. Rev. Lett. **92**, 163202 (2004).

[17] R. deCarvalho, J. Kim, J. D. Weinstein, J. M. Doyle, B. Friedrich, T. Guillet, and D. Patterson, Eur. Phys. J. D **7**, 289 (1999).

[18] M. Lara, J. L. Bohn, D. E. Potter, P. Soldán, and J. M. Hutson, Phys. Rev. A **75**, 012704 (2007).

[19] P. S. Żuchowski and J. M. Hutson, Phys. Rev. A **79**, 062708 (2009).

[20] S. Tokunaga, W. Skomorowski, R. Moszynski, P. S. Żuchowski, J. M. Hutson, E. A. Hinds, and M. R. Tarbutt, Eur. Phys. J. D (2011), DOI: 10.1140/epjd/e2011-10719-x.

[21] M. J. Seaton, Proc. Phys. Soc. London **88**, 801 (1966).

[22] M. J. Seaton, Rep. Prog. Phys. **46**, 167 (1983).

[23] C. H. Greene, U. Fano, and G. Strinati, Phys. Rev. A **19**, 1485 (1979).

[24] C. H. Greene, A. R. P. Rau, and U. Fano, Phys. Rev. A **26**, 2441 (1982).

[25] F. H. Mies, J. Chem. Phys. **80**, 2514 (1984).

[26] B. Yoo and C. H. Greene, Phys. Rev. A **34**, 1635 (1986).

[27] B. Gao, Phys. Rev. A **78**, 012702 (2008).

[28] S. Watanabe and C. H. Greene, Phys. Rev. A **22**, 158 (1980).

[29] F. H. Mies and P. S. Julienne, J. Chem. Phys. **80**, 2526 (1984).

[30] M. Raoult and G. G. Balint-Kurti, Phys. Rev. Lett. **61**, 2538 (1988).

[31] M. Raoult and G. G. Balint-Kurti, J. Chem. Phys. **93**, 6508 (1990).

[32] P. S. Julienne and F. H. Mies, J. Opt. Soc. Am. B **6**, 2257 (1989).

[33] J. P. Burke, C. H. Greene, and J. L. Bohn, Phys. Rev. Lett. **81**, 3355 (1998).

[34] F. H. Mies and M. Raoult, Phys. Rev. A **62**, 012708 (2000).

[35] M. Raoult and F. H. Mies, Phys. Rev. A **70**, 012710 (2004).

[36] B. Gao, E. Tiesinga, C. J. Williams, and P. S. Julienne, Phys. Rev. A **72**, 042719 (2005).

[37] Z. Idziaszek, T. Calarco, P. S. Julienne, and A. Simoni, Phys. Rev. A **79**, 010702 (2009).

[38] B. Gao, Phys. Rev. Lett. **104**, 213201 (2010).

[39] Z. Idziaszek and P. S. Julienne, Phys. Rev. Lett. **104**, 113202 (2010).

[40] Z. Idziaszek, G. Quéméner, J. L. Bohn, and P. S. Julienne, Phys. Rev. A **82**, 020703 (2010).

[41] B. Gao, Phys. Rev. Lett. **105**, 263203 (2010).

[42] J. M. Vogels, R. S. Freeland, C. C. Tsai, B. J. Verhaar, and D. J. Heinzen, Phys. Rev. A **61**, 043407 (2000).

[43] B. Gao, Phys. Rev. A **64**, 010701 (2001).

[44] B. Gao, Phys. Rev. A **58**, 1728 (1998).

[45] B. Gao, Phys. Rev. A **58**, 4222 (1998).

[46] B. Gao, Phys. Rev. A **80**, 012702 (2009).

[47] P. S. Julienne and B. Gao, AIP Conference Proceedings **869**, 261 (2006).

[48] R. G. Gordon, J. Chem. Phys. **51**, 14 (1969).

[49] B. R. Johnson, J. Comput. Phys. **13**, 445 (1973).

[50] M. L. González-Martínez and J. M. Hutson, Phys. Rev. A **75**, 022702 (2007).

[51] P. Soldán, P. S. Żuchowski, and J. M. Hutson, Faraday Discuss. **142**, 191 (2009).

[52] A. O. G. Wallis and J. M. Hutson, Phys. Rev. Lett. **103**, 183201 (2009).

[53] J. M. Hutson and S. Green, *MOLSCAT computer program, version 14*, distributed by Collaborative Computational Project No. 6 of the UK Engineering and Physical Sciences Research Council (2006).

[54] M. H. Alexander and D. E. Manolopoulos, J. Chem. Phys. **86**, 2044 (1987).

[55] B. Numerov, Publs. Observatoire Central Astrophys. Russ. **2**, 188 (1933).

[56] B. R. Johnson, J. Chem. Phys. **67**, 4086 (1977).

[57] J. M. Hutson, *BOUND computer program, version 5*, distributed by Collaborative Computational Project No. 6 of the UK Engineering and Physical Sciences Research Council (1993).

[58] I. Fourré and M. Raoult, J. Chem. Phys. **101**, 8709 (1994).

[59] K. M. Jones, E. Tiesinga, P. D. Lett, and P. S. Julienne, Rev. Mod. Phys. **78**, 483 (2006).